

Nucleation and growth of Si nanocrystals in an amorphous SiO₂ matrix

Daria Riabinina,^{1,*} Christophe Durand,¹ Joëlle Margot,² Mohamed Chaker,^{1,†} Gianluigi A. Botton,³ and Federico Rosei¹

¹*INRS-EMT, Université du Québec, 1650 Lionel-Boulet, C. P. 1020, Varennes Québec, Canada J3X 1S2*

²*Département de Physique, Université de Montréal, C. P. 6128, Succ. Centre-ville Montréal, Québec, Canada H3C 3J7*

³*Brockhouse Institute for Materials Research, Department of Materials Science and Engineering, McMaster University, Hamilton, Ontario, Canada L8S 4M1*

(Received 7 April 2006; revised manuscript received 20 June 2006; published 30 August 2006)

This paper discusses the physical mechanisms governing the nucleation and growth of Si nanocrystals embedded in an amorphous SiO₂ matrix. Reactive pulsed laser deposition combined with a postannealing treatment is shown to be a flexible approach to synthesize Si nanocrystals. This technique ensures an excellent control of Si nanocrystal size by varying the oxygen pressure. By correlating nanocrystal size (measured by x-ray diffraction and transmission electron microscopy) with the nonoxidized Si volume fraction (determined by x-ray photoemission spectroscopy), it is found that the formation of nanocrystals follows classical nucleation theory, whereby the average distance between nuclei centers remains constant.

DOI: [10.1103/PhysRevB.74.075334](https://doi.org/10.1103/PhysRevB.74.075334)

PACS number(s): 68.65.Hb

I. INTRODUCTION

Quantum confinement in nanostructures of indirect gap semiconductors has attracted great interest due to the changes in the electronic structure of these materials which significantly enhance their luminescence efficiency. After the first observation of visible photoluminescence (PL) from Si nanocrystals (Si-nc) at room temperature,¹ nanostructured semiconductors such as porous Si, Si nanoparticles, Si nanocrystals embedded in silicon oxide, and Si/SiO₂ superlattices have been intensively studied because of their potential optoelectronic applications.^{2–5} Among the various systems containing nanocrystals, silicon nanocrystals embedded in a Si oxide matrix are considered as one of the most promising since the available growth techniques allow a good control of nanocrystal size, size distribution, and density. To synthesize Si nanocrystals embedded in a silicon oxide matrix, Si-rich oxide films (SiO_x, 0 < x < 2) are deposited and then annealed at high temperature (usually above 1000 °C) to form nanocrystals by precipitation of Si excess in Si oxide matrix. Various techniques can be used for the fabrication of Si-rich oxide films, including ion implantation,⁶ chemical vapor deposition,⁷ laser ablation,⁸ and coevaporation.⁹

Several theoretical studies have been devoted to the understanding of crystal nucleation and growth in an amorphous matrix. Most of these investigations are based on the concept of surface tension.¹⁰ In contrast with the interface energy between a liquid medium and the smooth surface of a bulk solid, it is extremely difficult to measure the free interface energy between a crystalline nucleus and an amorphous matrix. Therefore, the main theoretical investigations on nucleation and growth in such systems were addressed by molecular-dynamics simulations with Lennard-Jones,¹¹ Stillinger-Weber,^{12,13} and Tersoff¹⁴ potentials. Despite the interest of these models for understanding the physical mechanisms governing nucleation and growth, there have been only a few comparisons between models and experimental data.¹⁵

On the other hand, from the experimental point of view, many studies have focused on the correlation between PL

and structural properties of Si nanoparticles.^{9,16,17} Amongst the key conclusions, it was demonstrated that the energy corresponding to the maximum of the PL spectrum shifts with nanoparticle size.⁹ However, the mechanisms governing the formation process of nanocrystals remain poorly understood.

One of the few experimental works dealing with the formation process of nanocrystals in an amorphous matrix after annealing was reported by Takeoka *et al.*¹⁸ who studied the size of Ge nanocrystals embedded in a Si oxide matrix as a function of the Ge volume concentration (also called volume fraction). By using a simple model for the Ge nanocrystal distribution, Takeoka *et al.* found that the interparticle distance was constant. However, these studies were performed in a narrow range of Ge volume fraction (3–7 % Ge), not permitting to develop a thorough physical interpretation of such observations.

The goal of the present work is to experimentally investigate the formation of Si-nc in a SiO₂ matrix, using a wide Si volume fraction range (1–65 %) to provide a complete description of the physical phenomena governing the formation of Si nanocrystals.

II. EXPERIMENT

Silicon-rich oxide films (SiO_x, 0 < x < 2) were deposited by reactive pulsed laser deposition (PLD) under low oxygen pressure (0.03–1.5 mTorr). This deposition technique is known for its capability to synthesize films with a well-controlled stoichiometry. In contrast with conventional PLD in an inert gas pressure,^{19–21} the use of oxygen in the ablation process of a Si target enables us to control the oxidation degree of silicon-rich oxide films.

A KrF excimer laser (wavelength 248 nm, pulse duration 17 ns, repetition rate 100 Hz) was used to ablate a Si rotating target (undoped Si wafer, purity 99.9999%). The laser fluence was set to 5 J/cm² (laser spot size 1.7 mm², laser power on the sample 1.2 W at 10 Hz, lens focal distance 1 m) and the substrate-target distance to 40 mm. Si wafers (covered with their native oxide) were used as substrates. The thickness of the deposited films was typically 400 nm,

as measured by imaging the sample's cross section by scanning electron microscopy. In our conditions, this corresponds to a deposition rate of 0.03 nm/pulse. After deposition, Si-rich oxide films were annealed for 1 h at a temperature of 1050 °C in an inert gas atmosphere (N_2). This thermal treatment constitutes a crucial step for the formation of Si nanocrystals. During annealing, Si atoms diffuse in the films to form Si nanocrystals by precipitation.

The structural properties of the deposited films were studied by x-ray photoelectron spectroscopy (XPS), x-ray diffraction (XRD), and transmission electron microscopy (TEM). XPS measurements were used to examine the oxidation process of ablated silicon as a function of the ambient oxygen pressure. XPS spectra of as-deposited SiO_x films were recorded using a monochromatic Al x-ray source ($h\nu = 1486.6$ eV) and an electron energy analyzer operating in the constant pass energy mode (20 eV). The photoelectron take-off angle was held at 90°. To remove the native oxide and organic surface contamination, the sample surface was sputtered by a 4 keV Ar ion beam (10 mA) for 10 min (etch rate ~ 5 Å/min). Due to the insulating properties of Si oxide, a slight shift of the XPS spectra due to charging was observed for the films deposited under high oxygen pressure. This effect was systematically corrected by positioning at 99.3 eV the Si 2*p* core level peak coming from nonoxidized silicon. XRD analysis was used to determine the size of Si nanocrystals embedded in the Si oxide matrix. XRD patterns were acquired at a grazing angle of 1° in the region of the Si (111) peak at $\theta = 28.3^\circ$. Raman spectra have been recorded at room temperature using the 514.5 nm line of an Ar ion laser as an excitation source. Finally, TEM measurements were carried out to estimate the size and distribution of Si nanocrystals. High resolution TEM (HRTEM) analysis was performed using a JEOL 2010F field emission TEM operated at 200 keV.²²

III. RESULTS

As reported previously,⁸ a significant PL signal depending on the oxygen pressure is emitted from the annealed SiO_x films. Photoluminescence occurs for samples synthesized under an oxygen pressure varying from 0.75 to 1.5 mTorr. The observed PL signal was attributed mainly to quantum confinement.⁸ In the present work, we focus on the influence of the oxygen pressure on the structural properties and composition of the SiO_x films.

A. XPS analysis

The dependence of the Si 2*p* XPS spectrum on the oxygen pressure is displayed in Fig. 1. The spectra were fitted with a Shirley background using the classical fitting approach involving five contributions corresponding to nonoxidized silicon Si^0 , as well as to the Si^{1+} , Si^{2+} , Si^{3+} , and Si^{4+} oxidation states.²³ As each Si atom forms four covalent bonds, the four oxidation states Si^{n+} (with $n=1-4$) are determined by the progressive oxidation of the Si atom (one O atom per covalent bond); therefore, Si^{4+} is associated with SiO_2 and Si^{1+} , Si^{2+} , Si^{3+} are related to Si-O suboxides. The relative position

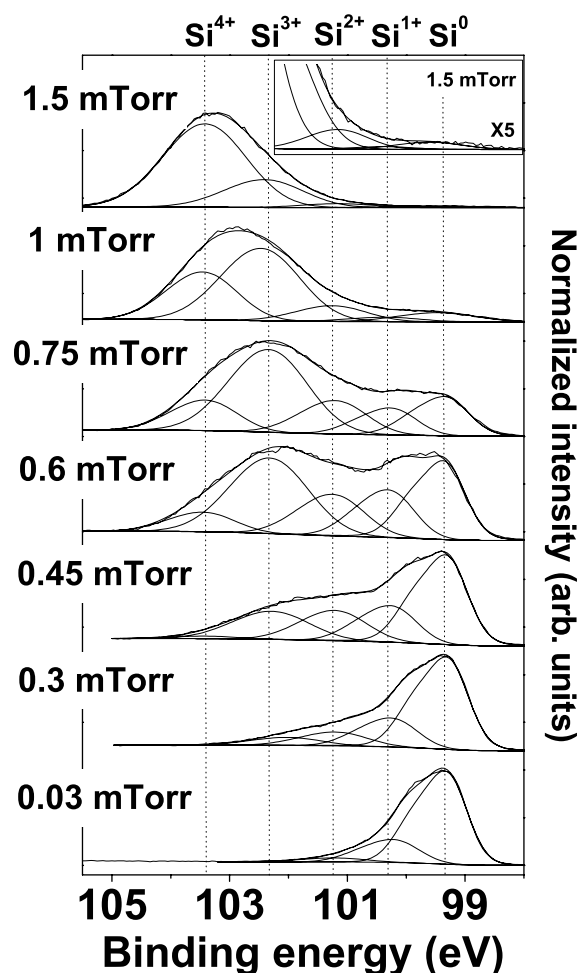


FIG. 1. Si 2*p* XPS spectra of as-deposited films for oxygen pressures varied from 0.03 to 1.5 mTorr (in the inset, the enlargement of the 1.5 mTorr sample is shown). All spectra were fitted with five peaks corresponding to silicon (Si^0), suboxide (Si^{1+} , Si^{2+} , and Si^{3+}), and SiO_2 (Si^{4+}) contributions.

and the full width at half maximum (FWHM) of all Si contributions were taken from the literature²⁴ and were fitted to the observed Si 2*p* spectra for all oxygen pressures, as shown in Fig. 1.²⁵

As expected, the degree of oxidation of the as-deposited SiO_x films (i.e., concentration of oxidized Si) progressively increases with increasing oxygen background pressure. At low O_2 pressure (0.03 mTorr), the Si 2*p* spectrum indicates that the film mainly consists of Si (peak maximum at 99.3 eV). The contributions at higher binding energy, resulting from silicon oxidation, gradually appear with increasing oxygen pressure. At the highest oxygen pressure investigated (1.5 mTorr), the films are thus mainly composed of SiO_2 (peak maximum at 103.3 eV). The Si 2*p* spectra demonstrate clearly the increasing oxidation of SiO_x deposited films with pressure. Indeed, the Si^0 contribution dominates the Si 2*p* signal at low oxygen pressure (77.9% of the total Si 2*p* spectrum area at 0.03 mTorr) and monotonously decreases as the pressure increases dropping to only 1.2% of the Si 2*p* total area at 1.5 mTorr. The intermediate oxidation states Si^{2+} and Si^{3+} become significant between 0.45 and 1 mTorr, while the

TABLE I. Si nanocrystal size d^{XRD} and Si volume fraction f_{Si^0} , obtained from XRD and XPS data, respectively, as a function of oxygen pressure P_{O_2} . The asterisks * indicate the photoluminescent samples.

P_{O_2} (mTorr)	FWHM (deg.)	d^{XRD} (nm)	C_{Si^0} (%)	f_{Si^0} (%)
0.03	0.71(\pm 0.02)	13.3(\pm 0.4)	78(\pm 8)	64(\pm 10)
0.08	1.01(\pm 0.05)	9.2(\pm 0.5)	68(\pm 7)	52(\pm 8)
0.15	1.22(\pm 0.08)	7.3(\pm 0.5)	68(\pm 7)	52(\pm 8)
0.3	1.40(\pm 0.13)	6.5(\pm 0.6)	62(\pm 6)	45(\pm 7)
0.38	1.65(\pm 0.15)	6.4(\pm 0.6)	47(\pm 5)	31(\pm 4)
0.45	1.59(\pm 0.18)	5.5(\pm 0.6)	43(\pm 4)	28(\pm 3)
0.6	1.8(\pm 0.2)	4.9(\pm 0.6)	25.5(\pm 2.5)	15.0(\pm 2)
0.75*	2.2(\pm 0.2)	4.2(\pm 0.4)	15.5(\pm 1.5)	8.7(\pm 1.0)
1*	2.3(\pm 0.3)	3.2(\pm 0.4)	6.3(\pm 0.6)	3.3(\pm 0.4)
1.25*	3.3(\pm 0.3)	2.6(\pm 0.3)	2.6(\pm 0.3)	1.4(\pm 0.2)
1.5*			1.2(\pm 0.2)	0.6(\pm 0.1)

silicon dioxide contribution (Si^{4+}) dominates at high pressure (72.5% of the Si $2p$ spectrum area at 1.5 mTorr). The non-oxidized Si concentration C_{Si^0} is defined by the area ratio of the Si^0 peak and the total Si $2p$ spectrum area, assuming the same electron escape depth for all Si $2p$ components.^{26,27} Its dependence on the oxygen pressure is shown in Table I. The increasing oxygen pressure results in a progressive charge transfer observed in the Si $2p$ spectra, since Si atoms progressively change the coordination with O atoms. The oxygen pressure determines the oxidation degree of SiO_x films, and consequently, the concentration of nonoxidized Si C_{Si^0} in the as-deposited films.

The Si^0 concentration can be linked to the relative volume occupied by Si nanocrystals in the deposited films by introducing the volume fraction of nonoxidized Si f_{Si^0} . The latter is defined as the ratio of the Si^0 volume V_{Si^0} to the total material volume V_{total} . The volume fraction f_{Si^0} can be estimated from XPS analysis according to

$$f_{Si^0} = \frac{V_{Si^0}}{V_{total}} = \frac{C_{Si^0}/\rho_{Si}}{C_{Si^0}/\rho_{Si} + (1 - C_{Si^0})/\rho_{SiO_2}}, \quad (1)$$

where ρ_{Si} and ρ_{SiO_2} are the Si and SiO_2 atomic volume densities, respectively.²⁸ The f_{Si^0} values deduced from XPS measurements are shown in Table I. As expected, the volume fraction of nonoxidized Si depends on the oxygen pressure and, thus, can easily be controlled by varying the oxygen pressure.

B. Nanocrystal size

The nanocrystal size was investigated by means of XRD and TEM analyses. Figure 2 shows the variation of the normalized (111) XRD peak for the annealed samples deposited at oxygen pressures varying from 0.03 to 1.25 mTorr, which corresponds to Si volume fractions between 1.4% and 64%. It is well known that PLD produces films with micron sized particles (also called droplets), that originate from the laser ablation process.^{29,30} The presence of droplets yields an in-

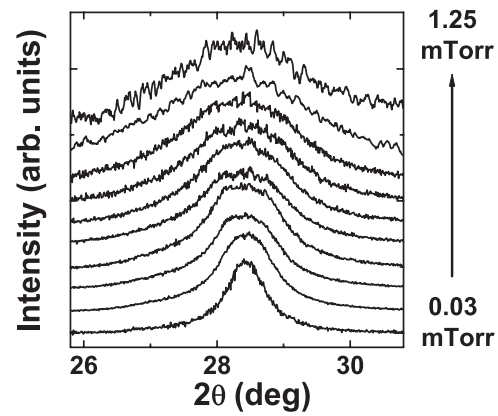


FIG. 2. Normalized (111) XRD spectra of Si nanocrystals as a function of oxygen pressure varied from 0.03 to 1.25 mTorr.

tense narrow XRD peak with a FWHM determined by both apparatus resolution and crystal quality. The droplet contribution (measured for as-deposited samples) was subtracted from the XRD spectra. The resulting XRD peak is shown in Fig. 2. The FWHM of the (111) XRD peak in the annealed films clearly increases with the oxygen pressure from 0.71° ($\pm 0.02^\circ$) at 0.03 mTorr to 3.3° ($\pm 0.4^\circ$) at 1.25 mTorr. The presence of Si nanocrystals causes a broadening of the XRD peaks, as shown in Fig. 2. Assuming the absence of nonuniform strain for nanosized Si crystals embedded in the amorphous Si oxide, the broadening of the XRD spectra can be attributed to the diminishing of Si nanocrystal sizes. Considering further the nanocrystals as perfectly spherical, their average size can be estimated using Scherrer's formula.^{31,32} The results are presented in Table I, which demonstrate that the oxygen pressure affects the average size of the Si-nc. The XRD peak could not be observed at an O_2 pressure of 1.5 mTorr because of low density and the small size of the Si nanocrystals. Since the XRD analysis is limited by the diffracting volume, this technique does not allow detecting very

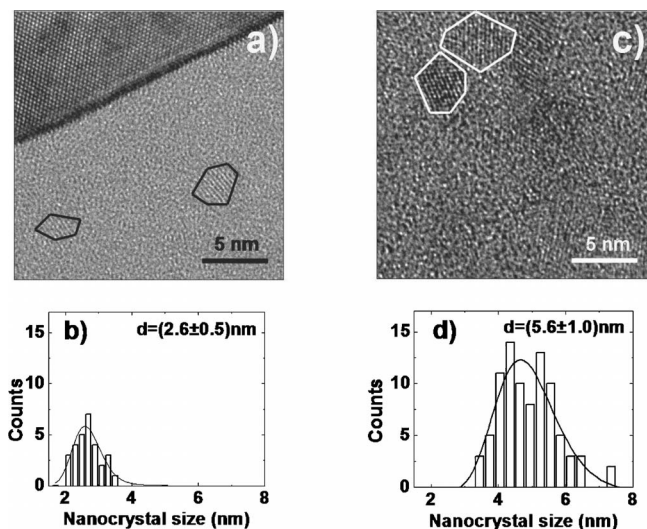


FIG. 3. Si nanocrystal HRTEM images and size histograms are shown for 3.3% (a) and (b) and 52% (c) and (d) Si^0 volume fraction samples.

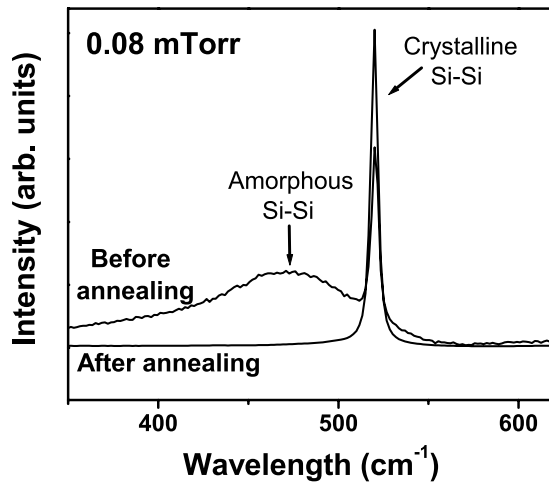


FIG. 4. Typical Raman spectra for samples deposited at 0.08 mTorr before and after annealing (1 h, 1050 °C).

small nanocrystals (<2 nm). Thus, the average nanocrystal size at 1.25 mTorr may be slightly overestimated.

To study the size distribution of Si nanocrystals, we performed cross-sectional HRTEM measurements of annealed samples. Figures 3(a) and 3(c) show the HRTEM images of Si nanocrystals embedded in Si oxide for samples corresponding to two Si volume fractions, namely 3.3% and 52%. Histograms corresponding to the nanocrystal size distribution for the same two samples are also shown in Figs. 3(b) and 3(d). The size distribution statistics are obtained from ~ 90 and ~ 30 nanocrystals for 52% and 3.3% Si volume fractions f_{Si^0} , respectively. The average nanocrystal size obtained from this HRTEM analysis was found to be 5.6 (± 1.0) nm for 52% f_{Si^0} and to 2.6 (± 0.5) nm for 3.3% f_{Si^0} .

IV. DISCUSSION

In the previous section, we have shown that the oxygen pressure determines the Si^0 volume fraction f_{Si^0} in the Si/SiO₂ system as well as the Si-nc size d^{XRD} . To understand the formation process of Si nanocrystals, we now discuss the relationship between f_{Si^0} and d^{XRD} based on our experimental results.

Correlating these two values is reasonable, since the value of f_{Si^0} calculated for the as-deposited samples can be considered as constant during annealing. Indeed, due to the weak diffusion coefficient of Si in silicon oxide (10^{-15} – 10^{-20} cm²/s, depending on oxygen concentration),³³ the nonoxidized Si contained in the 400-nm-thick films can neither migrate to the film surface (and be oxidized by the residual oxygen during the annealing) nor be supplied from the Si substrate. Moreover, to link the Si^0 volume fraction to the nanocrystal size, we have to ensure that f_{Si^0} describes the actual quantity of nonoxidized silicon forming nanocrystals. In this context, Raman spectroscopy and HRTEM analysis were used in order to make sure that amorphous Si and/or very small nanocrystals that cannot be detected by XRD were not present in the samples after annealing. Typical Raman spectra before and after annealing are shown in the Fig.

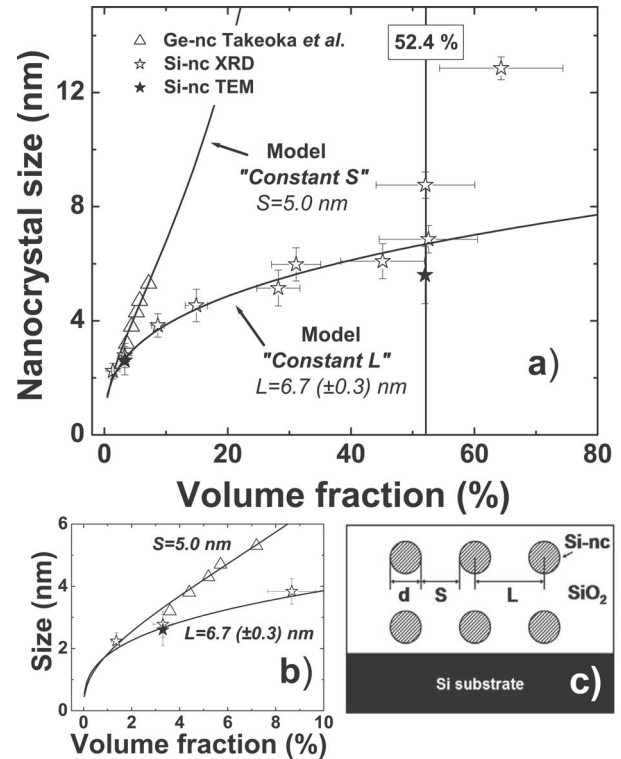


FIG. 5. Correlation between the Si nanocrystal core size and the Si^0 volume fraction. (a) Nanocrystal core size extracted from XRD and HRTEM data versus volume fraction obtained by XPS. (b) The enlarged graph for small volume fractions. Open triangles show the results obtained by Takeoka *et al.* for the Ge-nc/SiO₂ system. Open and solid stars show the results obtained in the present work by XRD and HRTEM, respectively. (c) Diagram of a simple cubic lattice model of distribution of Si nanocrystals in a Si oxide matrix.

4 for the samples deposited at 0.08 mTorr. The narrow Raman peak at 520 cm⁻¹ corresponds to Si-Si bonding in crystalline Si (Si substrate), whereas the large peak at 480 cm⁻¹ corresponds to the Si-Si bonding in amorphous Si. Figure 4 shows that the broad peak characterizing amorphous silicon disappears so that only the Si substrate peak remains observable after annealing. One can, therefore, conclude that the presence of amorphous silicon in the sample after annealing is negligible. According to the nanocrystal size distribution from HRTEM analysis [Figs. 3(b) and 3(d)], the presence of very small size nanocrystals (<2 nm) is also negligible and their concentration remains rather low at high oxygen pressures.³⁴ We also note that, to adequately correlate the Si^0 volume fraction to the nanocrystal size, an adjustment of this size needs to be performed. Indeed, Si nanocrystals are composed of a nonoxidized Si core of size d^{core} and of a Si-suboxide shell of thickness Δd^{shell} . On the other hand, the Si^0 volume fraction determined from XPS exclusively considers the Si-Si bonds (Si^0 contribution) located in the Si-nc core. Therefore, the correlation between the Si^0 volume fraction and nanocrystal size should exclude the shell contribution. In these conditions, the nanocrystal size thus reduces to the Si-nc core diameter d^{core} , calculated as $d^{\text{core}} = d^{\text{XRD}} - \Delta d^{\text{shell}}$. The thickness of the Si nanocrystal shell, Δd^{shell} , is estimated as $\Delta d^{\text{shell}} = 2 \cdot (1/2l_{\text{Si-O}} + 1/2l_{\text{Si-Si}}) \approx 0.4$ nm, where $l_{\text{Si-O}}$ and

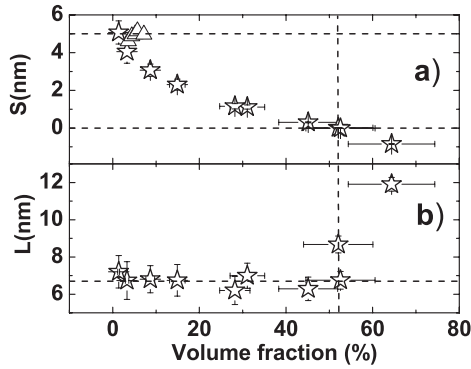


FIG. 6. Distances S and L between Si nanocrystals as a function of Si^0 volume fraction (stars). The data obtained by Takeoka *et al.* for Ge nanocrystals are shown for comparison (triangles).

$l_{\text{Si-O}}$ represent the Si-O and Si-Si bond lengths, respectively.^{35,36}

Figure 5(a) shows the Si nanocrystal core size d^{core} as a function of the nonoxidized Si^0 volume fraction varied in the range from 0% to 64%, while Fig. 5(b) shows an enlarged graph for small volume fractions (0–10%). Open and solid stars correspond to the present results as obtained by XRD and TEM. Open triangles are the data obtained by Takeoka *et al.* for the Ge-nc/ SiO_2 system.¹⁸ To fit their results, the authors proposed a simple model for the distribution of nanocrystals in a Si oxide matrix. The nanocrystals are assumed to be arranged in a simple cubic configuration with an interparticle distance S and a distance L between the centers of nanoparticles, as schematically shown in Fig. 5(c). From this model, the volume fraction f is related to the nanocrystal size d_{ave} by

$$\frac{f}{100} = \frac{4/3 \pi (d_{\text{ave}}/2)^3}{(d_{\text{ave}} + S)^3}. \quad (2)$$

Using this model, Takeoka *et al.* have determined a constant value of 5 nm for the interparticle distance S . Note, however, that this result is obtained for a limited range of volume fractions (3–7%).

As can be seen in Figs. 5(a) and 5(b), the model proposed by Takeoka *et al.* does not fit our experimental results. This means that, in the case of the Si-nc/ SiO_2 system, S is not constant. Instead, our results are well described if we assume that in Eq. (2) $L = d_{\text{ave}} + S$ is constant. In this case, the average size is expressed as

$$d_{\text{ave}} = L(6f/100\pi)^{1/3}, \quad (3)$$

where f is equal to the Si^0 volume fraction f_{Si^0} . The interparticle distance $S(f)$ [obtained from Eq. (2)] and the distance between the centers of particles $L(f)$ [obtained from Eq. (3)] as a function of volume fraction are shown, respectively, in Figs. 6(a) and 6(b). Clearly, our data cannot be fitted with a constant value of S [see Fig. 6(a)] but rather with a “constant L ” model for $f_{\text{Si}^0} = 1.4\text{--}52\%$ with $L \approx 6.7(\pm 0.3)$ nm [Fig. 6(b)]. However, above $f_{\text{Si}^0} = 52\%$, the “constant L ” model is

no longer valid. This is easily understood, since $f_{\text{Si}^0} = 52.4\%$ corresponds to the situation in which $L = d_{\text{ave}}$, i.e., $S = 0$ [as can easily be verified from Eq. (3)]. In this case, the nanocrystals come in contact. The drastic increase in the Si-nc size for $f_{\text{Si}^0} > 52\%$ could, therefore, be explained by interparticle coalescence, consistent with the fact that, based on XRD measurements, the nanocrystal size increases sharply to 13 nm for $f_{\text{Si}^0} > 52\%$, representing twice the Si-nc size at $f_{\text{Si}^0} = 52\%$. As shown in Figs. 5 and 6, the experimental data are well described by the model of a simple cubic lattice configuration. This model cannot be really supported by the HRTEM because this local technique only provides lattice-resolved images of the periodic structures oriented in the direction of observation. This model gives a macroscopic description of the uniform nanocrystal distribution, in which L is an average distance between the centers of nanocrystals.

To understand the physical phenomenon that yields a constant value of L in the Si-nc/ SiO_2 system, let us consider the main mechanisms governing the formation of Si nanocrystals in a Si oxide matrix. The size and spatial distribution of nanocrystals are determined by two basic mechanisms. The first one is diffusion that governs the system configuration through annealing temperature and time. The second one is related to the theory of nucleation and growth of nanocrystals in an amorphous matrix (discussed hereafter).

In the present work, the formation of Si nanocrystals in a Si oxide matrix occurs during annealing at 1050 °C for 1 h. At this temperature, we observed that the formation of Si nanocrystals is essentially completed. We have observed that the nanocrystal size grows when the temperature increases from 750 °C to 950 °C and remains stable above 950 °C (not shown here). Accordingly, we expect that the diffusion process ceases to play a role for temperatures higher than 950 °C. Therefore, after annealing at 1050 °C, the spatial distribution of Si nanocrystals should be uniquely determined by nucleation theory.

According to the classical theory of nucleation, the free energy related to the formation of nanocrystals with radius r in an amorphous matrix can be written as¹⁰

$$\Delta G_{\text{total}} = 4/3 \pi r^3 \Delta G_{\text{phase}} + 4 \pi r^2 \gamma \quad (4)$$

γ being the interface energy (i.e., the additional free energy per unit area associated with the boundary between nanocrystal and matrix) and ΔG_{phase} the difference in free energy between the nanocrystal phase and the matrix phase. For ΔG_{phase} negative, there exists a critical nanocrystal size

$$r^* = \frac{-2\gamma}{\Delta G_{\text{phase}}} \quad (5)$$

below which size shrinking is associated with a decrease of the total free energy. Such nanocrystals tend to reduce in size and vanish. On the other hand, for $r > r^*$, the nanocrystals must grow in size to reduce the total free energy. Such nanocrystals will either continue to grow or remain stable, but their center will not move. Note, however, that r^* cannot be estimated from Eq. (5) because obtaining reliable values for γ is extremely difficult.¹⁰

In the present work, the fact that the Si-nc spatial distri-

bution obeys the “constant L ” model for f_{Si^0} varying in the range of 1.4% to 52% can be associated with the nucleation regime in which the nuclei centers are in stable positions. We believe that, for $r < r^*$, the interparticle space should be constant (“constant S ” regime) and is determined by the diffusion coefficient of Si atoms in an amorphous matrix. The constant S regime is likely to occur when the Si nanocrystal size is smaller than 2 nm, which is the critical size r^* predicted theoretically.¹⁰

The results of Takeoka *et al.* show that in contrast with Si-nc in SiO₂, Ge nanoparticles in a SiO₂ matrix are characterized by S being constant. This could occur in two situations depending on whether the diffusion equilibrium in the system is reached or not. In the nonequilibrium case, the nanocrystals are not stable and the distance between the particles depends on the annealing parameters. At equilibrium state, when the size of nanoparticles remains smaller than the critical size described in nucleation theory, the constant S regime prevails. In both cases, the spatial organization of nanoparticles (i.e., nanoparticle size and internanoparticle distance) is mostly determined by the diffusion length of Ge atoms and could explain the difference between our data and Takeoka’s results.

V. CONCLUSION

We have synthesized Si nanocrystals embedded in a silicon oxide matrix using reactive PLD followed by a postan-

nealing treatment. This growth technique offers a great flexibility for tuning the nonoxidized Si concentration over a wide range (from 0.6% to 64%) by simply varying the oxygen pressure (from 1.5 to 0.03 mTorr). We found that the variation of nonoxidized Si concentration results in a change in the nanocrystal size from 2.6 to 13.3 nm. It is further shown that the formation of nanocrystals occurs according to classical nucleation theory, where the distance between the nuclei center remains constant for nonoxidized Si concentrations between 0.6% and 52%. We compared our results to those reported by Takeoka *et al.* for the Ge-nc/SiO₂ system. The behavior of the two systems differs, since for Ge-nc/SiO₂ the authors found the constant interparticle distance rather than a constant intercenter distance observed in our case. This discrepancy is likely to result from the differences between the diffusion characteristics and the free energy of the two systems.

ACKNOWLEDGMENTS

The authors would like to warmly thank D. Karpuzov, A. He, and S. Xu from ACSES (Alberta Center for Surface Engineering and Science) of the University of Alberta (Canada) for XPS measurements on the Kratos AXIS Ultra XPS spectrometer equipment. F.R., M.C. and G.B. acknowledge funding from Canada Research Chairs Program. M.C. and F.R. are grateful to FQRNT for partial support of this work. The authors are supported by NSERC of Canada.

*Corresponding author. Email address: riabinina@emt.inrs.ca

†Corresponding author. Email address: chaker@emt.inrs.ca

¹H. Takagi, H. Ogawa, Y. Yamazaki, A. Ishizaki, and T. Nakagiri, *Appl. Phys. Lett.* **56**, 2379 (1990).

²L. T. Canham, *Appl. Phys. Lett.* **57**, 1046 (1990).

³L. Pavesi, L. Dal Negro, C. Mazzoleni, G. Franzo, and F. Priolo, *Nature (London)* **408**, 440 (2000).

⁴D. F. Perepichka and F. Rosei, *Small* **2**, 22 (2006).

⁵M. De Crescenzi, P. Castrucci, M. Scarselli, M. Diociaiuti, P. S. Chaudhari, C. Balasubramanian, T. M. Bhavé, and S. V. Bhorkar, *Appl. Phys. Lett.* **86**, 231901 (2005).

⁶S. Guha, M. D. Pace, D. N. Dunn, I. L. Singer, *Appl. Phys. Lett.* **70**, 1207 (1997).

⁷D. Pacifici, G. Franzo, F. Priolo, F. Iacona, and L. Dal Negro, *Phys. Rev. B* **67**, 245301 (2005).

⁸D. Riabinina, C. Durand, M. Chaker, and F. Rosei, *Appl. Phys. Lett.* **88**, 073105 (2006).

⁹S. Takeoka, M. Fujii, and S. Hayashi, *Phys. Rev. B* **62**, 16820 (2000).

¹⁰J. K. Bording and J. Taftø, *Phys. Rev. B* **62**, 8098 (2000).

¹¹P. R. ten Wolde, M. J. Ruiz-Montero, and D. Frenkel, *J. Chem. Phys.* **104**, 9932 (1996).

¹²F. H. Stillinger and T. A. Weber, *Phys. Rev. B* **31**, 5262 (1985).

¹³P. Beaucage and N. Mousseau, *Phys. Rev. B* **71**, 094102 (2005).

¹⁴J. Tersoff, *Phys. Rev. B* **38**, 9902 (1988).

¹⁵M. C. Ridgway, G. D. Azevedo, C. J. Glover, R. G. Elliman, D. J. Llewellyn, A. Cheung, B. Johannessen, D. A. Brett, and G. J.

Foran, *Nucl. Instrum. Methods Phys. Res. B* **218**, 421 (2004).

¹⁶S. Guha, S. B. Qadri, R. G. Musket, M. A. Wall, and T. Shimizu-Iwayama, *J. Appl. Phys.* **88**, 3954 (2000).

¹⁷S. Guha, *J. Appl. Phys.* **84**, 5210 (1998).

¹⁸S. Takeoka, M. Fujii, S. Hayashi, and K. Yamamoto, *Phys. Rev. B* **58**, 7921 (1998).

¹⁹A. V. Kabashin, J.-P. Sylvestre, S. Patskovsky, and M. Meunier, *J. Appl. Phys.* **91**, 3248 (2002).

²⁰L. Patrone, D. Nelson, V. I. Safarov, M. Sentis, and W. Marine, *J. Appl. Phys.* **87**, 3829 (2000).

²¹C. Li, K. Kondo, T. Makimura, and K. Murakami, *Appl. Surf. Sci.* **197**, 607 (2002).

²²The samples were prepared in cross-section orientation by mechanical polishing followed by dimple grinding and low voltage argon ion milling (2 keV Ar final polish).

²³F. J. Himpsel, F. R. McFeely, A. Taleb-Ibrahimi, J. A. Yarmoff, and G. Hollinger, *Phys. Rev. B* **38**, 6084 (1988).

²⁴M. L. Green, E. P. Gusev, R. Degraeve, and E. L. Garfunkel, *J. Appl. Phys.* **90**, 2057 (2001).

²⁵The position shift was set at +0.9, +1.8, +2.6–3.0, and +4.0 eV for Si¹⁺, Si²⁺, Si³⁺, and Si⁴⁺ peaks, respectively, compared to the Si⁰ peak position. The FWHM was also set at 0.78, 0.9, 1.1, 1.2–1.4, and 1.2–1.5 eV for Si¹⁺, Si²⁺, Si³⁺, and Si⁴⁺ contributions, respectively. The Gaussian peak was chosen for Si¹⁺, Si²⁺, Si³⁺, and Si⁴⁺ contributions, while the Si⁰ peak was a Gaussian peak with 3% of Lorentzian shape.

- ²⁶Although the Si $2p$ electron escape depth $\lambda^{\text{Si } 2p}$ depends on the material, this variation should not affect the calculation of non-oxidized silicon concentration C_{Si^0} , because $\lambda^{\text{Si}^{2p}}$ is expected to be identical for all Si $2p$ components at a given oxygen pressure.
- ²⁷The uncertainty of quantitative XPS analysis is about $\pm 10\%$ [*Practical Surface Analysis*, 2nd ed, edited by D. Briggs and M. P. Seah (Wiley, Chichester, 1990), Vol. 1]. We have taken this uncertainty into account for nonoxidized concentration fraction C_{Si^0} and the corresponding error bar on Si⁰ volume fraction f_{Si^0} has also been considered (Table I).
- ²⁸The atomic volume densities ρ_{Si} and ρ_{SiO_2} were calculated using $\rho = Z/v$ and, where Z is the number of formulas in the unit cell and v is the volume of the elementary unit cell ($\rho_{\text{Si}} = 25.543 \text{ At/nm}^3$, $\rho_{\text{SiO}_2} = 49.944 \text{ At/nm}^3$).
- ²⁹E. Van de Riet, C. J. C. M. Nillesen, and J. Dieleman, *J. Appl. Phys.* **74**, 2008 (1993).
- ³⁰D. Riabinina, F. Rosei, and M. Chaker, *J. Exp. Nanosci.* **1**, 83 (2005).
- ³¹*Introduction to X-ray Powder Diffractometry*, edited by R. Jenkins and R. L. Snyder (Wiley, New York, 1996).
- ³²The measured FWHM of XRD peaks is equal to the sum of the FWHM corresponding to the nanocrystal size and the resolution of x-Ray diffractometer, equal to 0.2° .
- ³³V. A. Dan'ko, I. Z. Indutny, V. S. Lysenko, I. Yu. Madanchuk, V. I. Min'ko, A. N. Nazarov, A. S. Tkachenko, and P. E. Shepelyavy, *Semiconductors* **39**, 1197 (2005).
- ³⁴Assuming a log-normal distribution, the probability of the presence of very small particles ($< 2 \text{ nm}$) is equal to $\sim 6\%$ for samples deposited at 1 mTorr corresponding to the nanocrystal size of 2.6 nm [Fig. 3(b)]. For the sample deposited at 1.25 mTorr of oxygen, corresponding to the average nanocrystal core size of 2.2 nm, this probability cannot be neglected. Therefore, for this pressure, the correlation between the XRD measurement and XPS data is not straightforward.
- ³⁵J. C. Aubry, T. Tyliczszak, A. P. Hitchcock, J.-M. Baribeau, and T. E. Jackman, *Phys. Rev. B* **59**, 12872 (1999).
- ³⁶R. A. B. Devine and J. Arndt, *Phys. Rev. B* **35**, 9376 (1987).